Thermal Assessment of the PTC System in Arid Algerian Regions

H. Daoui[a], S. Tlili[b], A. Kaddour[c], Y. Menni[d], L. Benmebrouk[a], M. Said. Nedjimi[e]

[a] Univ. Ouargla, Fac. Mathematics and Material Sciences, Lab. Radiation and Plasmas and surface Physics Laboratory (LRPPS), 30000, Ouargla, Algeria

[b] Univ. Ouargla, Fac. Mathematics and Material Sciences, Lab. Development Of New And Renewable Energies In Arid And Saharan Zones Laboratory (LARENZA), 30000, Ouargla, Algeria

[c] Unité de Recherche Appliquée En Energie Renouvlables, URAER, Centre de Devlopement des Energies Renouvlables, CDER, 47133, Ghardaia, Algeria

[d] Ctr. Univ. Naama, Fac. Department of Technology, 45000, Naama, Algeria

[e] Univ. Ouargla, Fac. Mathematics and Material Sciences, Lab. Valorisation and Promotion of Saharan Resources Laboratory (VPRS), 30000, Ouargla, Algeria

Email corresponding author: tlilisalah2007@gmail.com

Received: 07/ 2023; Published: 08/ 2023

Abstract :

In this work, the calculation was used to see the evolution of the maximum daily intensity of direct solar radiation, the duration of sunshine, and the maximum air temperature during the year in the regions of 'El Oued and Ghardaïa (Algeria). In order to choose the days when the values of these values are the lowest in each region, in order to study the evolution of the output of a cylindrical parabolic solar concentrator. We have found that less than 0.6 W/m^2 in maximum radiation intensity difference and 0.01 h difference in sunshine duration are sufficient to only last for two days instead of three. , the first of which is the winter solstice and the second is the fourth day of the year. We were also able to follow, during the two days of study, the evolution of the intensity of direct solar radiation, the temperature of the air, the temperature of the water leaving the solar concentrator, the quantity of heat energy absorbed, whether instantaneous or total, and finally the total heat return.

We have noticed that the shape of the evolution of the first four is generally in the form of a parabola, while the evolution of the last two is differentiated from them by their symmetry, regardless of the school day and its region. There is no significant difference between the two study areas, although the Ghardaïa region is often the highest. While the yield is higher in the

valley region, the latter is not affected by a change of study day as long as there is a rapprochement between them. The highest values of these coefficients are; (697.31 W/m2, 04/01, Ghardaïa), (21.87 °C, 22/12, Ghardaïa), (54.82 °C, 22/12, Ghardaïa), (7.08 kW, Ghardaïa), (166.41 MWD, 04/ 0 01, Ghardaïa), (81.67%, 12/22, El Oued), respectively.

Key words: solar radiation, air temperature, linear parabolic solar concentrator, outlet temperature, absorbed heat energy, thermal efficiency.

Tob Regul Sci.™ 2023;9(1): 4056-4073
DOI: doi.org/10.18001/TRS.9.284

Introduction

The most often applied technique in solar plants to produce electricity and in industrial and thermal processes is the parabolic trough collector (PTC) [1-3]. The concentrator and the receiver tube are significant components of the solar field. The reflector surface of the concentrator reflects solar rays onto the receiving tube, which converts solar power into heat transmitted to the heat transfer fluid (HTF), such as air, water, or oil [4]. The receiver comprises a selective-coated metallic tube to enhance the absorption of solar irradiance.

Allam et al. 2022 [1] indicated that the helical shaft insert had increased the required pumping power for the same flow rate. However, the parabolic trough collector thermal performance has enhanced with the shaft rotational speed.Rafiei et al. 2020 [5] revealed that the highest optical performance was attained when the cavity was placed at the PTC focal line. Moreover, it is found that there is an optimum cavity aperture area to determine the greatest thermal efficiency.

Saad et al. 2022 [6] showed that the heat transfer characteristics of rectangular fins with round edge are better than those with sharp edge in solar parabolic trough collector.Wang et al. 2016 [7] showed that the optical efficiency of PTCs changes from 0.4 to 0.8 in a whole year. The highest optical efficiency of PTCs is in June and the lowest is in December. The optical efficiency of PTCs is mainly influenced by the solar incidence angle. The main objective of the present work is to evaluate the performance of the PTC concentrator in the two arid Algerian sites of Ghardaia and El Oued, respectively.

PTC System design

The studied PTC is schematized in the following picture:

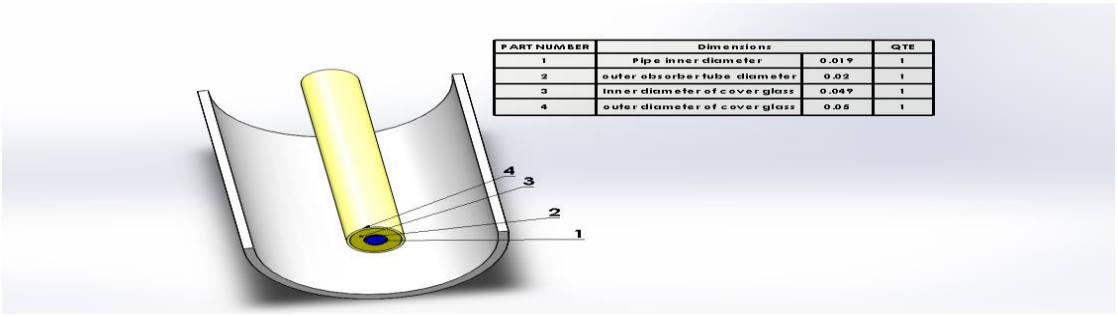

Figure 1: The design of the studied solar concentrator

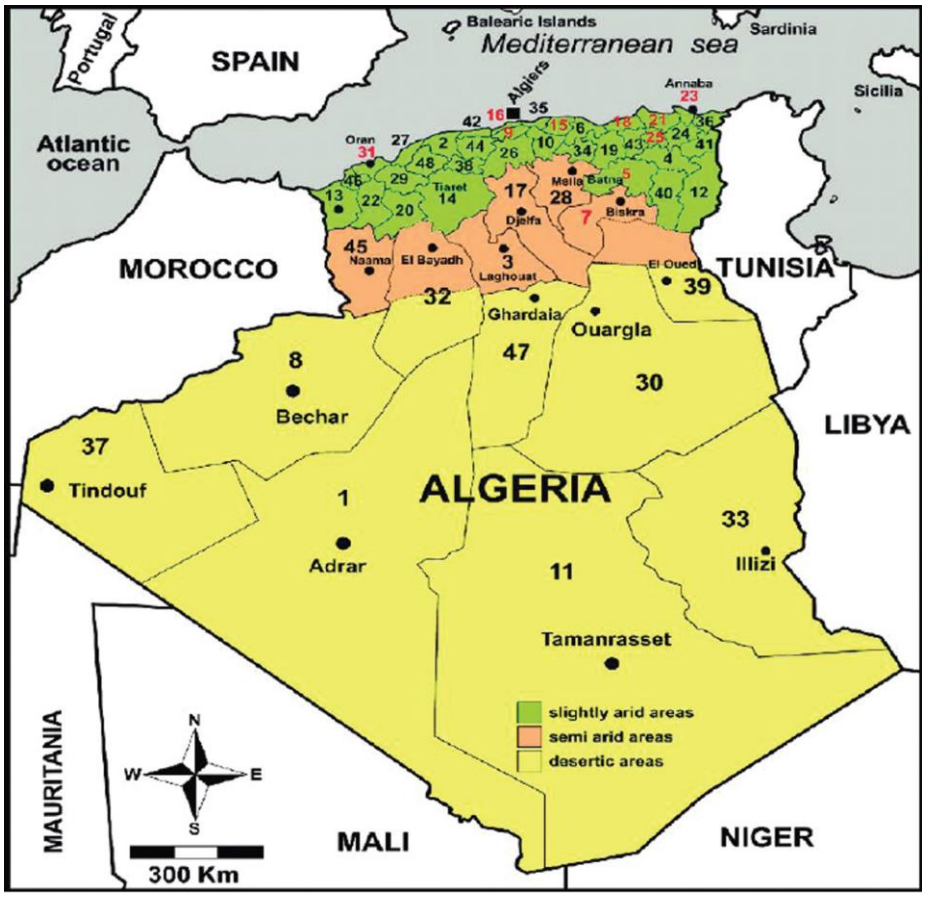

Figure 2: Geographical site for the 2 case studies [8]

Methodology

To achieve the objectives of this study, the following steps must be followed, which we try to present briefly due to its length:

1- Determine the intensity of direct radiation:

In the arid regions, as are the three study regions, the total radiation intensity is equal to the direct radiation.

This intensity is calculated from; the three topographic values, which are: longitude, latitude, and height above sea level. And as its value changes daily, it is definitely related to the number of the day of the year, i.e. the number of the day of the month and the number of the month of the year, and it is determined for the sake of our study as it comes later. To calculate this severity based on one of the several models, among which the work presented: [9-11].

2- Determine the absolute temperature of the region and the temperature of the sky:

The actual observed temperatures can be used, as can be calculated using the [12] follows:

$$T_a = \left(\frac{T_{a(max)} - T_{a(min)}}{2}\right)\cos\left(\frac{(14-t)\pi}{12}\right) + \left(\frac{T_{a(max)} + T_{a(min)}}{2}\right)$$

Where Ta (max) Ta (min) are the maximum and minimum ambient temperatures per month in the study area, t is the local time previously calculated when calculating the intensity of direct radiation.

Table (1): The values of the astronomical lcation of the study area. [13,14]

	El Oued	Ghardaïa
Alti	76	445
Lati	33.43	32.386
Long	6.9	3.794

Table (2): The values of the maximum and minimum monthly temperatures for the two study areas. [13, 14]

	El Oued		Ghardaïa	
	Tmax	Tmin	Tmax	Tmin
JANNUARY	16.89	08.95	20.03	08.69
FEBRUARY	20.16	08.83	25.24	14.26
MARCH	34.35	17.87	30.22	14.93
APRIL	33.93	21.66	32.19	21.43
MAY	39.12	25.48	37.56	24.81
JUNE	46.28	31.41	42.09	29.07
JULY	46.15	33.67	42.69	34.15
AUGUST	42.71	31.60	40.53	30.87
SEPTEMBER	42.80	29.27	39.70	28.97
OCTOBER	30.88	21.05	36.22	25.31

NOVEMBER	32.11	18.17	27.99	14.06
DÉCEMBER	20.84	10.30	21.87	10.68

If we adopt the highest and lowest absolute temperature tables for each month, which are specific to each region (see tables 1 and 2).

The sky temperature can now be calculated according to the Garcia-Valladares et al. relation Velazquez, 2009[15]:

$$T_{sky} = 0.0552 {T_a}^{1.5}$$

3- Determining the study days:

Based on the results of the previous two steps, it is theoretically possible to find the following days for each of the study areas:

- The day when the maximum intensity of direct solar radiation is the highest compared to other days.

- The day when the intensity, duration, or time of insolation is the highest compared to other days.

- The day when the total intensity of direct solar radiation is the highest compared to other days.

- The day when the ratio of the total intensity of solar radiation to the time of insolation is the highest compared to that of other days.

- Today, the maximum air temperature value is the highest compared to other days.

Today, the maximum sky temperature is the highest compared to other days.

4- Calculating the useful heat and instantaneous efficiency of the solar collector:

Installation of the concentrator: As is known, the linear concentrator consists of a cylindrical reflector with a cross-section in the form of a parabola (width w = 3 m), in the concentrator of the cut, a tube (length L = 5 m) is fixed, and it is made of copper, called the absorbent element, and it is hollow so that the fluid can pass through it (water). In our work, we assume that this tube is covered with glass of both thicknesses, that is, an internal diameter and an external one. It is represented in the figure below:

Greater detail is described in the work of [16]

Before addressing the theoretical aspect, in particular, of the thermal balance of heat transfer in the three parts that make up the concentrator, and in order for this concentrator to be somewhat ideal and to be simpler to study, the following hypotheses must be fulfilled:

- Uniformity in temperature distribution at the level of the heat-collecting element is acceptable, given that the glass envelope is not vacuumed.

- Neglecting the thickness of the surfaces as it is very small compared to the dimensions of the concentrator.

- Heat transfer is one-dimensional, that is, heat exchanges take place in the diagonal direction, and thus there is no difference between the different cross-sections of the heat-collecting element. According to Forristal [17], who points out that this assumption can be accepted for PTC systems smaller than 100 m in length.

The system is considered to be thermally stable.

- There is no phase change of water during flow inside the absorbent tube.

Considering that the solar tracking is complete, ignore the errors of the solar tracking.

Considering the optical and thermal properties of various materials (coefficients: reflection, absorption, transmission, and thermal conductivity) independent of temperature.

The theoretical principle of determination: Generally, according to the aforementioned structure, when the solar radiation falls on the reflector, the rays focus on the receiver, which is represented by the glass cover. To absorb part of it by absorbing the energy of the photons of radiation by the material, to increase the vibrations of its atoms to increase its temperature, Te. Leaving part of it to receive from the end of the absorbent tube, which absorbs part of the heat with the same mechanism to increase its temperature. Part of it is delivered by convection to the working fluid as useful heat Tf. But in fact, the matter is more complicated, as the heat depends in its transfers here on all the usual mechanisms represented in; Transmission by conduction, transmission by convection and transmission by radiation. Where the receptors' absorption of solar radiation must be high, and the energy loss by all these mechanisms must be low.

After thermal equilibrium for each part of the core, we obtain its differential equation. After simplifying this equation using finite differences, for a time period of one second, we get the following equations Marif et al., 2014[18]:

a- The equation for the glass envelope:

$$\rho_G A_G C_{pG} {T_G}^{t-\Delta t}(j) + (IC_g \rho^{\circ} \alpha_G + (h_{CvGa} T_a + h_{RGS} T_S))\pi D_{Ge} = (\rho_G A_G C_{pG} + \pi((h_{CvGO} + h_{RGO})D_{Gi} + (h_{CvGa} + h_{RGS})D_{Ge})){T_G}^{t}(j) - ((h_{CvGO} + h_{RGO})\pi D_{Gi}){T_O}^{t}(j)$$

b- The equation for the absorbent tube:

$$\rho_O A_O C_{pO} {T_O}^{t-\Delta t}(j) + IC_g \tau_G \alpha_O \rho^{\circ} \pi D_{Oe} = -(h_{CvGO} + h_{RGO})\pi D_{Oe} {T_G}^{t}(j) + \left(\rho_O A_O C_{pO} + \left((h_{CvGO} + h_{RGO)})D_{Oe} + h_{CvOf} D_{Oi}\right)\pi\right){T_O}^{t}(j) - h_{CvOf} D_{Oi} \pi {T_f}^{t}(j)$$

c- Equation for the fluid:

$$\dot{m}_f C_{pf} {T_f}^{t}(j-1) = -h_{CvOf} \Delta x D_{Oi} \pi {T_O}^{t}(j) + \left(\dot{m}_f C_{pf} + h_{CvOf} \Delta x D_{Oi} \pi\right){T_f}^{t}(j)$$

Where AO and AG are calculated as follows:

$$A_O = \frac{\pi}{4}(D_{Oe}^2 - D_{Oi}^2)$$

and

$$A_G = \frac{\pi}{4}(D_{Ge}^2 - D_{Gi}^2)$$

Also, Δx is calculated from the following relation:

$$\Delta x = v_f \Delta t = \frac{4\dot{m}_f \Delta t}{\pi D_{Oi}^2 \rho_f}$$

The time required for the amount of water to pass through each absorbent tube is:

$$\tau = \frac{L}{v_f} = \frac{L}{\Delta x}\Delta t = \frac{L}{\Delta x}$$

Δt = 1 s

.

As for the average efficiency of the concentrator or the yield, it is defined as the ratio of the energy flow gained to the ratio of the radiation energy falling on the concentrator. As stated in the work of [13]. It is calculated from the following relationship:

$$\eta(\%) = 100\frac{\sum \dot{Q_u}}{L.w\sum I}$$

Results and Discussions

Determination of study days

To determine the study days in this work, preference was given to examining the evolution of the maximum intensity of direct solar radiation, the duration of insolation, and the highest air temperature during the year in the two study areas. These developments are respectively represented in figs. 3(a andb), and 4(a). By providing a general overview of the first two figures, it is evident that there is a significant agreement in the evolution of the maximum intensity of direct solar radiation and the duration of insolation between the two study areas. This could be attributed to the convergence of latitude between the two regions, as indicated in table 1, where the difference is estimated at 1.056.

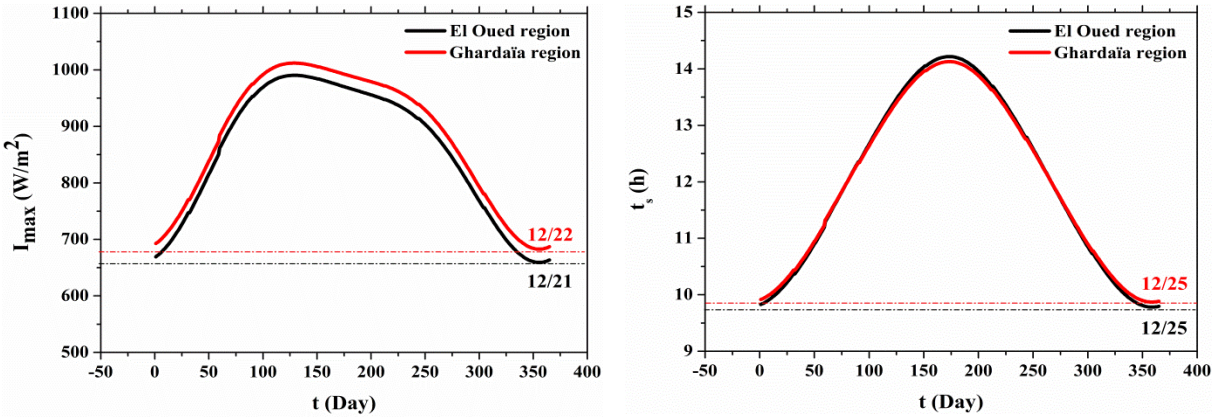

(a) (b)

Figure 3.Daily variations in the (a) maximum intensity of direct solar radiation, (b) duration of insolation, throughout the year in the two study areas.

Based on fig. 3(a), it is evident that the maximum intensity of direct solar radiation exhibits a strong and linear increase from December 22nd for the Ghardaïa region and December 21st for the El Wadi region. This upward trend continues until nearly May 5th, when the maximum intensity reaches its peak in both regions. Subsequently, a gradual and semi-linear decrease occurs until around early August. The starting point of this significant decrease aligns with the point where the increase begins again, as previously mentioned. Hence, December 22nd for Ghardaïa and December 21st for El Wadi mark the days with the lowest maximum intensity of solar radiation in the two regions. Additionally, Ghardaïa consistently experiences slightly higher values compared to the other region, as observed in table 3. This slight disparity could be attributed to the impact of longitude, with an estimated difference of 3.606 (refer to table 1).

Regarding fig. 3(b), it is evident that the changes in the duration of insolation throughout the year follow an almost parabolic pattern. Notably, the duration of insolation only increases from December 25th until the beginning of June in both study areas. This increase is rapid and nearly linear. Subsequently, the rate of increase slows down until April 24th, when the duration of insolation reaches its maximum values in both areas. From this point onward, a gradual and

almost linear decrease begins until July 19th, when a rapid decrease ensues until the point of increase, as mentioned earlier. Thus, December 25th marks the day with the least amount of insolation for both regions. In terms of the Ghardaïa region, its values are slightly lower than those in the valley region only during the period between the spring solstice (March 21st) and the autumn solstice (September 23rd). During this period, the duration of insolation in Ghardaïa is eight minutes and 24 seconds longer, as indicated in table 3. This slight difference may also be influenced by longitude.

Almost every month, regardless of the studied area, reveals that the Ghardaïa region consistently exhibits higher values, except for January, February, October, and December. In these specific months, the difference is minimal, estimated to be approximately one degree (calculations can be derived from table 2. However, in January, our calculations indicate that the lowest maximum air temperatures occur on the second day for Ghardaïa and the fourth day for El-Wadi, measuring 20°C and 17°C respectively (as shown in table 3).

The table 3 demonstrates that the disparity in maximum solar radiation intensity between December 21st and December 25th in the Valley region, as well as between December 22nd and 25th in the Ghardaia region, is insignificant, with values of up to 0.59 W/m2 and 0.56 W/m^2 respectively. Thus, these differences and the slight variation between consecutive days, such as 21st and 22nd, can be disregarded. Considering that the 22nd represents the winter solstice, it is preferable to choose it in this case. Similarly, the fourth day of January can be selected to represent the lowest duration of sunshine in both study areas. Likewise, the fourth of January serves as an appropriate representation for the lowest maximum atmospheric temperature in the two study areas, based on the same rationale.

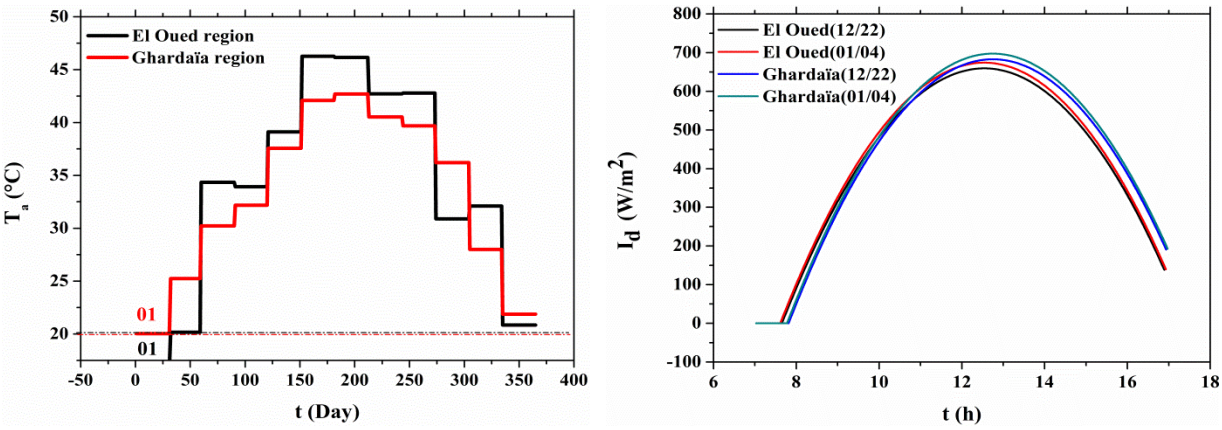

(a) (b)

Figure 4.(a) Daily variations in the maximum air temperature throughout the, (b) momentary variations of direct solar radiation in the two study areas on two specific days.

Studying the evolution of climate variables

Studying the evolution of direct solar radiation intensity

This phenomenon is depicted in fig. 4(b), illustrating the logical progression of all curves from non-existent values to the onset of direct solar radiation within a short time span. The duration of these periods is estimated at approximately 32 minutes on the fourth day of January and around 33 minutes on the twenty-second day of December in the Valley region. In the Ghardaïa region, the duration is approximately 45 minutes on both study days, following the same order as previously mentioned (refer to table 4). Additionally, due to its eastern location, the valley region experiences sunrise 10 and 9 minutes earlier than the Ghardaïa region, respectively corresponding to the two study days. Irrespective of the study day, the Ghardaïa area exhibits higher intensity values of this radiation shortly before eleven o'clock.

The variation in the intensity of direct solar radiation and the length of the day follows a parabolic pattern. Notably, there is a clear correlation between these intensities when the study day changes within the same area, particularly before nine in the morning and after four in the evening. The fig. 4(b) provides further evidence supporting this observation. Moreover, it is evident that the decline in intensity during sunset exhibits different values, with a close proximity in sunset times varying by two minutes within the same area and by three minutes on the same day.

In terms of radiation intensity, the Ghardaïa region consistently demonstrates higher values, surpassing the others by 53.07 W/m^2 and 52.55 W/m^2 respectively in the previous consecutive study days. Furthermore, the peak intensity in this region exceeds the others by 23.35 W/m^2 and 23.51 W/m^2 within the same series. This pattern consistently shows a higher initial change in the valley, which gradually diminishes after eleven o'clock.

Study of the evolution of absolute air temperature

The fig. 5(a) represents the variations in air temperature during the two study days in both regions. It is evident that this change is similar between the two study regions and within each region, albeit with a slight difference. The magnitude of this difference increases as we progress towards the peak of the temperature change and decreases as time approaches sunset. Similar to the change in the intensity of direct solar radiation, this temperature change follows a parabolic pattern, albeit with a more open shape.

At sunrise, the temperature values are estimated as follows: (12.93 °C, 04/01) and (14.91 °C, 12/22) for Ghardaïa and the valley region respectively on the first study day, and (11.96 °C, 04/01) and (14.35 °C, 12/22) on the second study day, in the same respective regions. These values are notably lower compared to the temperature values at sunset, which are (18.40 °C, 04/01) and (20.30 °C, 12/22) in Ghardaïa and the valley region respectively on the first study

day, and (15.78 °C, 04/01) and (19.40 °C, 12/22) on the second study day, again in the same respective regions.

The apex of this temperature segment is approximately reached around the second hour in the past, following the same sequence, and possesses the following values: (20.03 °C, 04/01), (21.87 °C, 12/22), (16.89 °C, 04/01), and (20.84 °C, 12/22).

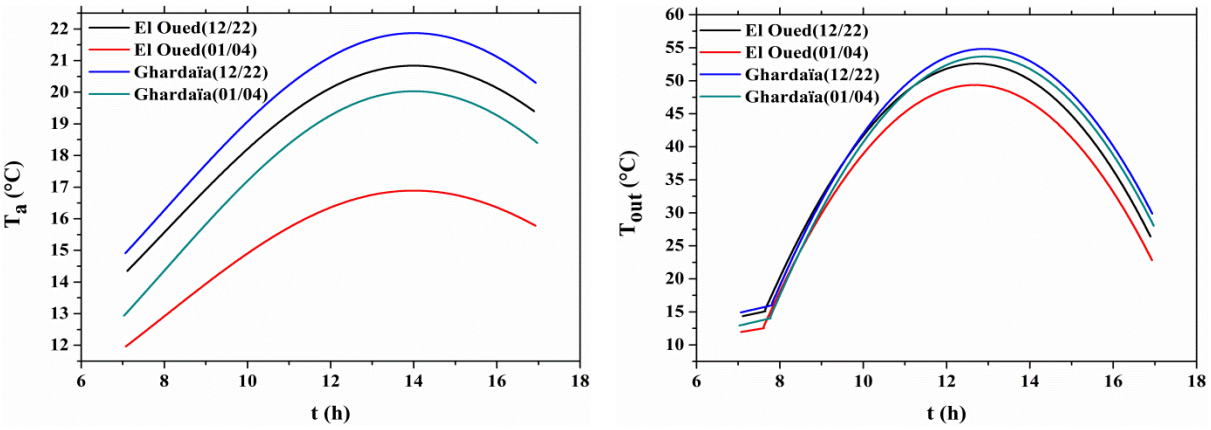

(a) (b)

Figure 5.Instantaneous variations of (a) air temperature, (b) water temperature exiting the solar concentrator, on two specific days in the two study areas.

Studying the development of the outputs of the solar concentrator

Study of the change in the water outlet temperature

The variations in the exit temperature over the two study days in both regions are depicted in fig. 5(b). It is observed that this change closely resembles the fluctuations in air temperature. Since the water temperature was not non-existent during the period without direct solar radiation, it was assumed that the water entered the system at the same air temperature. The table 4 records the exit temperatures at the moment of radiation arrival as follows: (14.30 °C, 04/01), (16.28 °C, 12/22), (12.78 °C, 04/01), and (15.37 °C, 12/22).

Regarding the highest values, which typically occur after midday, approximately fifty-four minutes in the Ghardaïa region (occurring at the same time on both study days) and forty minutes in the Valley region, the temperatures are as follows: (53.66 °C, 04/01), (54.82 °C, 12/22), (49.35 °C, 04/01), and (52.58 °C, 12/22). At sunset, the temperatures are recorded as (28.03 °C, 04/01), (29.86 °C, 12/22), (22.83 °C, 04/01), and (26.42 °C, 12/22). These results confirm that the water temperature has a greater impact compared to radiation intensity, as indicated by the varying magnitudes of heat between the two regions. Additionally, it can be

observed that the water temperature in the valley region is higher than in the other region only before nine and ten o'clock on January 4th and December 22nd, respectively.

Study of the instantaneous absorbed thermal energy change

The fig.6(a) illustrates the instantaneous change in thermal energy absorbed from the water over the two study days in both regions. It is evident that this change closely corresponds to the variations in the intensity of direct solar radiation. Prior to the arrival of radiation, the thermal energy is non-existent as the exit temperature is equal to the entry temperature, which is equivalent to the air temperature.

Furthermore, the order of the values remains consistent, following the pattern of radiation intensity change (refer to fig. 4(b)) in all the aspects mentioned earlier. However, there is a slight variation in the timing of values exceeding those of the Ghardaia region, which begin at ten o'clock instead of eleven o'clock. Notably, there is an increasing convergence between the values of the two study days in the Valley region, while a clear correspondence is observed in the Ghardaia region. These findings reinforce the significant influence of air temperature, as supported by the results presented in table 4.

The peak values of this thermal energy occur minutes after midday, with a slight delay in the Valley region compared to the Ghardaia region. Specifically, in the successive study days, the highest values are estimated as follows: (7.08 kW, 04/01), (7.08 kW, 12/22), (6.84 kW, 04/01), and (6.70 kW, 12/22). At sunset, the respective values are: (2.01 kW, 04/01), (2.18 kW, 12/22), (1.47 kW, 04/01), and (1.47 kW, 12/22), maintaining the same order.

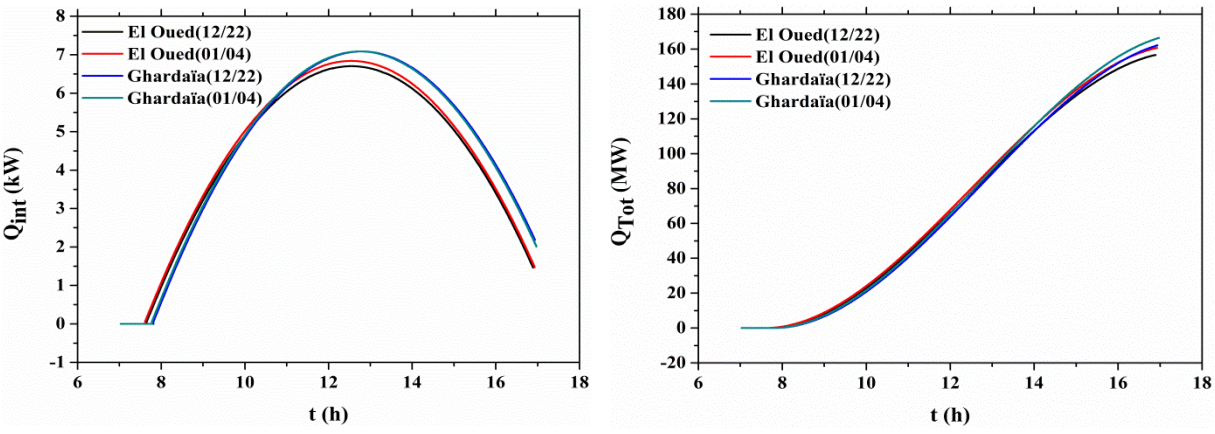

(a) (b)

Figure 6. The instantaneous changes in the (a) absorbed energy, (b) total energy, from the solar concentrator during the two study days in the two study areas.

Study of the change of total absorbed thermal energy

The fig.6(b) illustrates the temporal increase in the total absorbed energy, starting from non-existent values at sunrise until the onset of direct solar radiation. From that moment until around 9 in the morning and from 3 in the afternoon until sunset, the increase is gradual and non-linear. However, from 9 to 3 in the afternoon, the increase follows a linear pattern. The values of this energy are very close, particularly before 2 in the afternoon, especially within the same region. Before this time, the valley region consistently leads the Ghardaia region, while after this time, the situation is reversed, resulting in a diminishing convergence. These results are reflected in the values presented in table 4, where the total energy in the Ghardaïa region on the fourth day of January is estimated at 166.41 MW, exceeding its value on December 22nd by 4.25 MW and surpassing the values in the Valley region by 5.69 MW and 9.76 MW, respectively, in the same order as the two study days.

Study of the total heat yield change

The fig.7 demonstrates the variations in heat yield throughout the two study days in both regions, exhibiting a similar pattern to the overall change in total absorbed energy, albeit with notable distinctions. Notably, the heat yield in the valley region consistently surpasses that of the Ghardaia region before sunset, following a parabolic trend. Furthermore, the total return remains unaffected by the specific study day, as evidenced by the correspondence between its values and the day of observation.

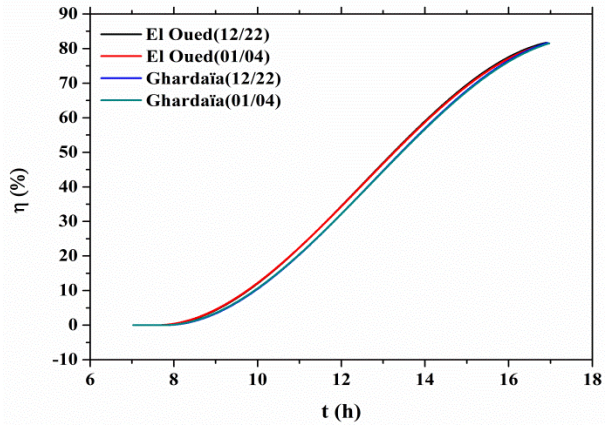

Figure 7. Instantaneous changes in total heat return in the two days and two study areas.

Conclusions

Based on the results of this study, several key points can be deduced. Firstly, there is a consistent agreement regarding the annual variations in the maximum intensity of direct solar radiation and the duration of sunshine between the two study areas, which are situated at the same latitude. However, slight deviations are observed due to differences in longitude and elevation above the Earth's surface.

The selection of study days based on the lowest solar radiation intensity or the shortest duration of tan does not provide significant additional insights. The differences between these factors in the two regions are not substantial, making it sufficient to choose just one of them. Alternatively, selecting the coldest day of the year based on air temperature could be a suitable criterion.

The shape of the changes in solar radiation intensity and the two outlets of the cylindrical parabolic solar concentrator (represented by outlet temperature and absorbed thermal energy) exhibit similar patterns. However, the ambient temperature also plays a crucial role, as it influences the order of the resulting values.

Furthermore, the overall evolution of total heat energy absorbed and total thermal efficiency follows a consistent pattern, with minimal variations based on the selected study days.

Most of the results demonstrate close agreement between the two study regions and the chosen day, as the differences observed are negligible and not statistically significant.

This work opens up several avenues for further research. It is possible to explore additional parameters for determining study days. Additionally, incorporating experimental values for solar radiation intensity and air temperature at the beginning of simulations could improve accuracy, considering the various influencing factors like cloudiness, dust, wind speed, and wind direction.

While challenging, a fully experimental approach can be pursued, particularly when it involves solar tracking with concentrators of this nature.

Finally, conducting an annual study to capture data throughout the year would provide a comprehensive understanding, as the selection criteria in this study were based on the lowest values, leaving room for exploring potential improvements on other days.

References

[1] Allam, M.; Tawfik, M.; Bekheit, M.; El-Negiry, E. Experimental Investigation on Performance Enhancement of Parabolic Trough Concentrator with Helical Rotating Shaft Insert. Sustainability 2022, 14, 14667. https://doi.org/10.3390/su142214667

[2] Fernández-García, A.; Zarza, E.; Valenzuela, L.; Pérez, M. Parabolic-TroughSolarCollectors and Their Applications. Renew. Sustain. EnergyRev. 2010, 14, 1695–1721.

[3] Anabela, E.; Panduro, C.; Finotti, F.; Largiller, G.; Yngve, K. A Review of the Use of Nanofluids as Heat-Transfer Fluids in Parabolic-Trough Collectors. Appl. Therm. Eng. 2022, 211, 118346.

[4] Abed, N.; Afgan, I. An Extensive Review of Various Technologies for Enhancing the Thermal and Optical Performances of Parabolic Trough Collectors. Int. J. EnergyRes. 2020, 44, 5117–5164.

[5] Rafiei, A., Loni, R., Ahmadi, M. H., Najafi, G., Bellos, E., Rajaee, F., &AskariAsli-Ardeh, E. (2020). Sensitivity analysis of a parabolic trough concentrator with linear V-shape cavity. Energy Science & Engineering, 8(10), 3544-3560.

[6] B Saad, N., MM Abdala, A., &Fatouh, M. (2022). Thermal Enhancement of Parabolic Trough Collectors using Absorber Tubes with Internally longitudinal Round Edge Fins. Engineering Research Journal, 173, 356-375.

[7] Jinping Wang, Jun Wang, Xiaolong Bi, Xiang Wang, "Performance Simulation Comparison for Parabolic Trough Solar Collectors in China", International Journal of Photoenergy, vol. 2016, Article ID 9260943, 16 pages, 2016. https://doi.org/10.1155/2016/9260943

[8] Kaddour A, El HadiAttia M, Arıcı M, Benbelgacem K, Driss Z. A numerical evaluation on the utilization of earth to air heat exchangers in arid regions Algeria. J TherEng 2022;8(4):505–514.

[9] Capderou. M, 1987. Atlas Solaire de l'Algerie, Modeles Théoriques et Expérimentaux. Volume1, Tome 2 ; Office des Publications Universitaires, Algérie

[10] Kasten.F,1996. The linke turbidity factor based on improved values of the integral rayleigh optical thickness. SolarEnergy 56 (3), 239–244.

[11] Louche. A, Peri. G, Iqbal. M,1986. An analysis of Linke turbidity factor, Solar Energy 37 (6), 393-396.

[12] Trabelsi.A, Masmoudi.M, 2011. An investigation of atmospheric turbidity over Kerkennah Island in Tunisia. AtmosphericResearch 101, 22–30.

[13] Ghardaia region. (n.d.). Retrieved june 13, 2023, from https://www.weatherbase.com/weather/weather.php3?s=592472&cityname=Ghardaia-Ghardaia-Algeria

[14] Oued region. (n.d.). Retrieved june 13, 2023, from https://www.weatherbase.com/weather/weather.php3?s=599065&cityname=El-Oued-El-Oued-Algeria

[15] Garcia-Valladares, O, Velazquez. N, 2009. Numerical simulation of parabolic trough collector: improvement using counter flow concentric circular heat exchangers. International journal of heat and mass transfer 52 (3/4), 597–609.

[16] Wang Fuqiang, Cheng Ziming, Tan Jianyu, Yuan Yuan, Shuai Yong, Liu Linhuab, 2017, Progress in concentrated solar power technology with parabolic trough collector system: A comprehensive review, Renewable and Sustainable Energy Reviews 79 (2017) 1314–1328

[17] R. Forristall, "Heat transfer analysis and modeling of a parabolic trough solar receiverimplemented in engineering equation solver," National Renewable Energy Laboratory, 1617Cole Boulevard, Golden, Colorado, 80401-3393, Tech. Rep. NREL/TP-550-34169,October2003.

[18] Marif.Y, Benmoussa. H, Bouguettaia. H, Belhadj. M. M, Zerrouki. M, 2014. Numerical simulation of solar parabolic trough collector performance in the Algeria Saharan region. Energy Conversion and Management 85, 521–529

Nomenclature

	Ambienttemperature	T_a	01
	Monthly maximum air temperature	$T_{a(max)}$	02
	Monthly minimum air temperature.	$T_{a(min)}$	03
	Skytemperature	T_s	04
	The temperature of the fluid or water.	T_f	05
	The temperature of the absorbent part.	T_o	08
	The temperature of the glass cover.	T_c	11
	Initial fluid temperature.	T_{fi}	12
	The final fluid temperature.	T_{ff}	13
	The electrical resistance corresponding to heat transfer by convection between the absorbent element and the fluid.	R_{cof}	14
	The electrical resistance corresponding to heat transfer by convection between the glass cover and the absorbent element.	R_{cco}	15
	Electrical resistance corresponding to convectional heat transfer between the atmosphere and the glass envelope.	R_{cac}	16
	The electrical resistance corresponding to heat transfer by radiation between the absorbent element and the fluid.	R_{rco}	17
	The electrical resistance corresponding to heat transfer by radiation between the sky and the glass envelope.	R_{csc}	18
	Heat transfer coefficient by convection between the absorbent element and the fluid.	h_{cof}	19
	Heat transfer coefficient by convection between the glass envelope and the absorbent element.	h_{cco}	20
	Heat transfer coefficient by convection between the atmosphere and the glass envelope.	h_{cac}	21

	Radiation heat transfer coefficient between the absorbent element and the fluid.	h_{rco}	22
	Radiation heat transfer coefficient between the sky and the glass envelope.	h_{csc}	23
	The amount of heat absorbed by the fluid.	Q_f	24
	The amount of heat absorbed by the absorbent element.	Q_o	25
	-The amount of heat absorbed by the glass envelope.	Q_c	26

0.05	Mass flow rate in the concentrator pipe (kg/s).	$\dot{m}_f$	01
5	Concentrator length (m)	L	02
3	Concentrator width (m).	w	03
0.019	Inner pipe diameter (m).	D_{oi}	04
0.02	External absorbent tube diameter (m).	D_{oe}	05
4185	Specific heat capacity of water (W/m2).	C_{pf}	08
1000	Water density (kg/m^3)	ρ_f	11
8940	The absorbent element's density (kg/m^3).	ρ_o	12
2530	Glass density (kg/m3)	ρ_c	13
0.97	Absorbency of the absorbent element..	α_o	14
0.05	Absorbency of the glass cover.	α_c	15
0.935	The permeability of the glass cover.	τ_c	16
40	Geometric focus of radiation.	C_g	17
0.935	Reflection coefficient.	ρ^0	18
0.1	The emission factor of black chrome	ε_o	19
0.9	Emission factor	ε_c	20

$3.66 * 10^8$		σ	21
1		γ^*	22
1	Normal pressure	a	23